Theranostics

DOI: 10.1002/anie.201400133

An MRI-Sensitive, Non-Photobleachable Porphysome Photothermal Agent**

*Thomas D. MacDonald, Tracy W. Liu, and Gang Zheng**

Abstract: *Photothermal therapy makes use of photothermal sensitizers and laser light to thermally ablate diseased tissues. Porphysome nanoparticles offer a nontoxic alternative to inorganic nanocrystals for the efficient conversion of light into heat. Mn^{3+} ions were incorporated directly into the building blocks of our porphysome nanoparticles, thus imparting MRI sensitivity while simultaneously improving photostability and maintaining high photothermal efficiency. Mn porphysomes are as photothermally effective as free-base porphysomes and can rival gadolinium diethylenetriaminepentaacetate (Gd-DTPA) for MRI contrast generation. Their MRI contrast generation, photothermal efficiency, and photostability are unprecedented for an all-organic nanoparticle composed of a single functional component.*

Photothermal therapy (PTT) is an emerging treatment modality in which the controlled generation of heat is utilized to ablate diseased (i.e. cancerous) tissues.[1] Heat is generated through the interaction of laser light with photothermal agents, which are able to mediate the conversion of light into heat. Heating is localized to the areas in which the photothermal agent and applied light overlap, thus giving excellent spatial control and preventing excessive off-target damage.[1b,2] This provides two distinct means to localize photothermal damage to target tissues: modulating the accumulation of the photothermal agent and directing light administration.

Nanomedicine, the application of nanotechnology to medicine, aims to selectively deliver molecular cargo to diseased tissues, and as such, it forms a natural fit with PTT. Nanoparticles have a number of strengths; too large to be cleared through the renal system, they have prolonged circulation times, thus extending their exposure in vivo.[3] Additionally, they are capable of escaping circulation at sites where the vasculature becomes irregular, such as in tumours, thereby selectively accumulating in diseased tissue through the enhanced permeability and retention (EPR) effect.[4] Seeking to exploit this effect has driven the field of nanomedicine, and nano-enabled PTT has received its fair share of attention. The most common PTT agents are gold nanoparticles (GNPs).[5] GNPs have excellent photothermal efficiency and photostability but are not biodegradable, thus leading to concerns about their long-term fate and safety in vivo.[6] An alternative exists in porphysomes: nontoxic (no toxicity in mice up to 1000 mg kg^{-1}), biodegradable, all-organic nanoparticles with photothermal properties comparable to that of gold.[7] Being comprised of organic dyes however, porphysomes can potentially photobleach under irradiation, which is a concern for PTT.[5b] Improving the photostability of porphysomes would therefore be of benefit to porphysome PTT. The other method for controlling PTT damage is through the directed application of light. For PTT, light is typically applied through laser fibres. Positioning of the laser fibres is of the utmost importance to maximize the deposition of energy in target tissue while minimizing off-target heating. Imaging modalities can be used to direct this placement if it is possible to detect the diseased tissue in real-time or near-real-time.[8] Modalities such as ultrasound and MRI have been utilized previously in conjunction with contrast agents to good effect.[9] This is where the capabilities of nanomedicine again shine through; they provide a platform for combining diagnostic and therapeutic components into a single theranostic agent.[10] Combining contrast and photothermal agents into a single entity would allow the direct visualization of agent accumulation to guide light application and predict treatment effects. Porphysomes, already inherently multimodal, offer an attractive platform upon which to build a theranostic PTT agent owing to their high payload of porphyrins.[7b] The porphyrin moieties within porphysomes are capable of directly chelating metal ions so they can be stitched directly into the fabric of the nanoparticle without having to add any exogenous components.[7b,11] We have previously shown that porphysomes are strong chelators of metal ions that can stably incorporate radioactive copper-64 for PET imaging.[11] We can exploit this capability to chelate paramagnetic Mn^{3+} ions, which are able to generate contrast in MRI.[12] By labelling all 80000 porphyrins in each porphysome, we can create a potent, high-payload contrast agent. Herein, we demonstrate an approach to adding MRI contrast to the porphysome construct, thus adding capacity for image-guidance without increasing the complexity of the system. Additionally, this approach synergistically improves

[*] T. D. MacDonald, Dr. T. W. Liu, Prof. G. Zheng
Ontario Cancer Institute and Techna Institute, UHN (Canada)
E-mail: gang.zheng@uhnres.utoronto.ca
T. D. MacDonald, Prof. G. Zheng
Department of Pharmaceutical Sciences
University of Toronto (Canada)
Dr. T. W. Liu, Prof. G. Zheng
Department of Medical Biophysics
University of Toronto (Canada)

[**] We would like to thank Dr. Warren Foltz for assistance with MR imaging, Shawn Stapleton for assistance with photoacoustic imaging, Dr. Jon Lovell and Mojdeh Shakiba for assistance with TEM imaging, and Laura Burgess for assistance with the MTT assay. Funding was provided by OICR, NSERC, CIHR, CFI, the Princess Margaret Cancer Foundation, and the Joey and Toby Tanenbaum/Brazilian Ball Chair in Prostate Cancer Research.

Supporting information for this article is available on the WWW under http://dx.doi.org/10.1002/anie.201400133.

 © 2014 Wiley-VCH Verlag GmbH & Co. KGaA, Weinheim

the photostability and photothermal aspects of Mn porphysomes over free-base porphysomes, thus providing a method for generating potent MRI-detectable photothermal agents.

The conversion of pyropheophorbide-lipid (pyro-lipid) to Mn pyro-lipid (Figure 1 A) was fast (≤ 2 h) and quantitative, as previously reported,[13] and the product was easily integrated into existing porphysome methodologies. Mn porphysomes formed liposome-like nanovesicles similar to those of

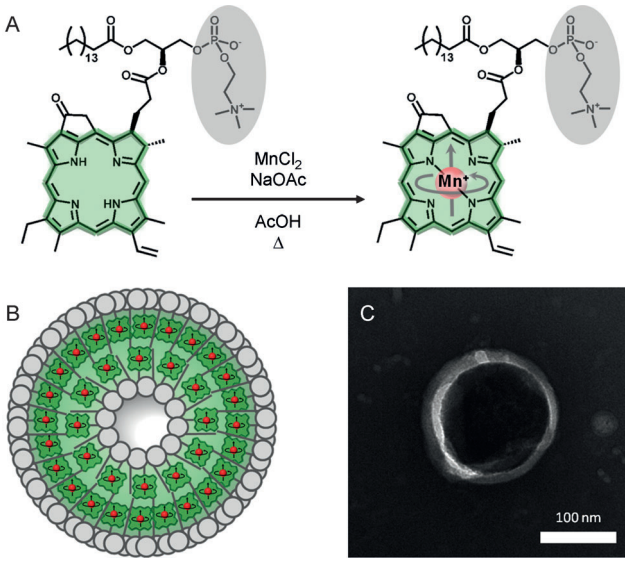

Figure 1. A) Synthetic method for inserting Mn into pyro-lipid. B) Schematic representation of Mn-porphysome nanovesicles (not to scale). C) Representative TEM of Mn-porphysome nanoparticles (scale bar 100 nm).

free-base porphysomes as shown by transmission electron microscopy (TEM; Figure 1 B Figure 1 C and Figure S1 in the supporting Information). Some heterogeneity in electron attenuation by the membrane (which contains only Mn pyro-lipid and DSPE-PEG) is observed in the micrograph, possibly a result of demetalation of Mn caused by the harsh conditions of uranyl acetate staining [low pH, high osmolality; DSPE = distearoylphosphatidylethanolamine, PEG = poly(ethylene glycol)]. Dynamic light scattering (DLS) of the Mn porphysomes utilized in this study showed monodisperse populations (PDI < 0.2) with average sizes between 120–130 nm (Figure S2B, a representative batch showing a z average of 123.4 nm and PDI of 0.159). Mn porphysomes were also well tolerated by KB cell cultures (viability $> 90\%$) in concentrations up to 50 μM as determined by MTT assay (Figure S3). Unlike free-base pyro-lipid, Mn pyro-lipid has an axial acetate ligand orthogonal to the plane of the porphyrin. The fact that this group did not sterically disrupt the formation of the porphysome architecture shows that the porphysome platform has a degree of resilience, thus indicating that structural changes to the porphyrin moiety can be tolerated. This opens the door to the inclusion of different metal ions.

To evaluate the MRI detectability imparted by the inclusion of the Mn^{3+} ions, relaxivity values were determined for both intact and disrupted Mn porphysomes at 7T in solution on a 96-well plate (Figure 2 A, B). A plot of inverse relaxation time versus concentration showed ionic relaxivity values of $r_1 = (1.2 \pm 0.2)$ mM^{-1}s^{-1} and $r_2 = (7.0 \pm 0.5)$ mM^{-1}s^{-1} when intact and $r_1 = (4.0 \pm 0.3)$ mM^{-1}s^{-1} and $r_2 = (12.9 \pm 0.5)$ mM^{-1}s^{-1} when disrupted by detergent. These values

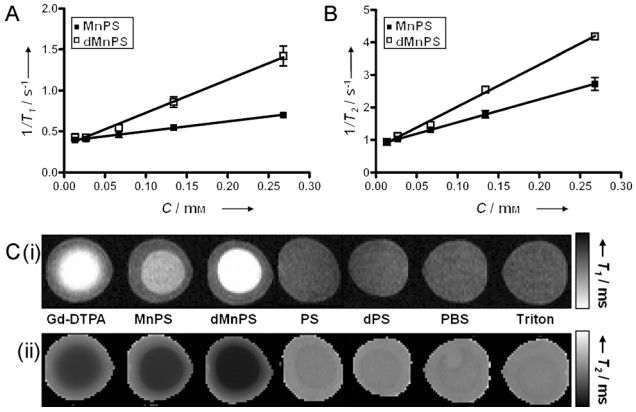

Figure 2. Inverse relaxation plots for calculating r_1 (A) and r_2 (B) of Mn porphysomes (MnPS) and detergent-disrupted Mn porphysomes (dMnPS). C) T_1 (i) and T_2 (ii) maps of two-layer polyacrylamide gel phantoms containing Gd-DTPA, intact and disrupted Mn porphysomes, intact (PS) and disrupted (dPS) free-base porphysomes, PBS, and Triton detergent in their inner layers. Gd-DPTA = gadolinium diethylenetriaminepentaacetate.

correspond to estimated per particle relaxivities of $r_1 = (96\,000 \pm 16\,000)$ mM^{-1}s^{-1} and an $r_2 = (560\,000 \pm 40\,000)$ mM^{-1}s^{-1} while intact, increasing to $r_1 = (3200\,000 \pm 24\,000)$ mM^{-1}s^{-1} and an $r_2 = (1032\,000 \pm 40\,000)$ mM^{-1}s^{-1} upon disruption. These values reveal disrupted Mn porphysomes to be comparable to the routinely used Gd-DTPA for generating MRI contrast, as shown in the two-layer gel phantoms (Figure 2 C). The relaxation times of the inner portion of the phantoms showed statistically significant differences between detergent-disrupted Mn porphysomes (dMnPS) and both Mn porphysomes (MnPS) and Gd-DTPA, but not between MnPS and Gd-DTPA in the T_1 manifold. In the T_2 manifold, there were statistically significant differences between the relaxation times of all three active agents (Figure S3.1). The increase in relaxivity upon disruption of Mn porphysomes (2.8-fold for r_1, 1.8-fold for r_2) is likely the result of increased water access to the inner coordination shell of the Mn ions that are otherwise couched within the hydrophobic bilayer. This structural dependence opens the door for dissociation-driven signal enhancement. Structurally quenched fluorescent nanoparticles, including free-base porphysomes, have been shown to exhibit dissociation-driven signal amplification in response to pH changes or receptor-mediated cell uptake,[14] and a similar method could be used to "turn on" the Mn-porphysome MRI signal. This approach would likely require active targeting to increase the rate of cell uptake, which would require further study but makes Mn porphysomes an attractive candidate for MRI molecular imaging.

The insertion of Mn^{3+} into the porphyrin ring quenched the ability of Mn porphysomes to generate reactive oxygen

 © 2014 Wiley-VCH Verlag GmbH & Co. KGaA, Weinheim

species (ROS; Figure 3A). Mn porphysomes also show a marked enhancement in photostability over free-base porphysomes. Irradiation of free-base porphysomes for a total of 5 min at 750 mW cm^{-2} photobleached all but $<20\%$ of the Q-band absorbance (Figure 3B). By contrast,

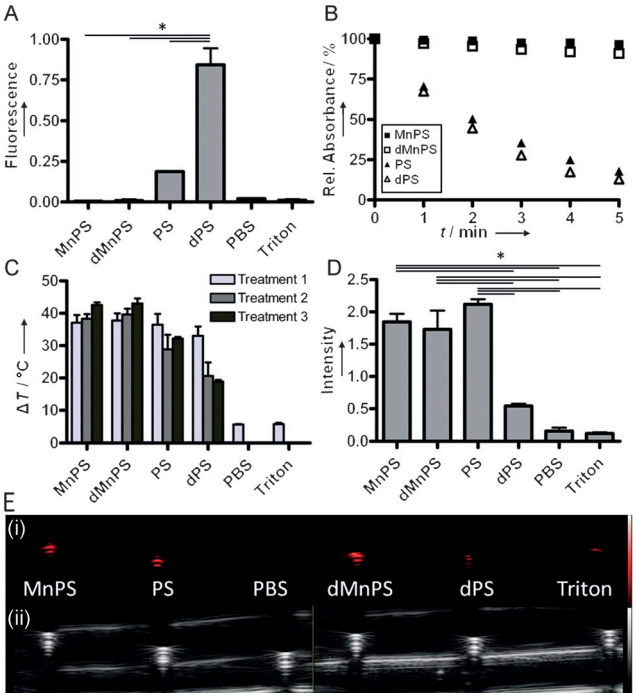

Figure 3. Characterization of the photonic properties of Mn porphysomes. A) Singlet-oxygen generation by porphysomes after 1 min of laser irradiation (671 nm, 100 mW cm^{-2}) as quantified by singlet oxygen sensor green (SOSG) fluorescence ($n=3$). B) The photostability of porphysomes during high power (750 mW cm^{-2}) laser irradiation as indicated by relative absorbance at 680 nm over time ($n=3$). C) Change in temperature at the end of two consecutive 5 min photothermal treatments (680 nm laser, 750 mW cm^{-2}) ($n=3$). D) Relative photoacoustic intensity ($n=3$). E) representative photoacoustic (i) and ultrasound (ii) images of porphysomes in tube phantoms (680 nm excitation). * $p<0.05$.

Mn porphysomes maintained $>95\%$ of the Q-band absorbance under the same irradiation regimen. These effects are two sides of the same coin. The insertion of paramagnetic ions into porphyrins drastically decreases their excited-state lifetimes, thus funnelling excited states into nonradiative decay paths and concurrently reducing the opportunities for self-destructive photochemistry or photosensitization.[15] This quenches the porphyrins photochemistry intramolecularly, thereby causing the Mn porphysomes to act purely in the photothermal mode, regardless of the state of the supramolecular nano-assembly. This loss of structural dependence relative to free-base porphysomes can be seen in the photoacoustic imaging of Mn and free-base porphysomes (Figure 3D,E). Mn porphysomes do not exhibit any loss of photoacoustic signal following disruption with detergent while the photoacoustic signal of the free-base porphysome drops 4-fold upon disruption. The enhancement in photostability bears itself out in the ability to perform repeated photothermal treatments on the same sample without loss in heat production (Figure 3C). Solution photothermal experiments show that Mn porphysomes, whether intact or disrupted, did not lose photothermal capacity over three sequential photothermal treatments (raising solution temperatures by (37 ± 5) °C, (38 ± 3) °C, and (43 ± 1) °C while intact and (38 ± 5) °C, (40 ± 4) °C, and (43 ± 2) °C when disrupted, under 680 nm irradiation at 750 mW cm^{-2} for 5 min). Free-base porphysomes lost capacity as a result of photobleaching with each treatment (raising the temperature by (36 ± 8) °C, (28 ± 11) °C, and (32 ± 1) °C while intact and (33 ± 7) °C, (20 ± 10) °C, and (19 ± 1) °C when disrupted). Given that Mn porphysomes are so difficult to photobleach, Mn porphysome PTT is both reliable and reproducible, thus simplifying situations requiring repeated treatments.

The approach of utilizing paramagnetic ions to generate MRI contrast and streamline photonic properties shows promise, although there are some avenues open for further refinement. An entirely different paramagnetic ion/chelator pair could be used, such as gadolinium and texaphyrin.[16] Gadolinium has more unpaired electrons than manganese, so coupled with the high-payload nature of porphysomes, it has the potential to make a potent MRI agent. Additionally, the lipid chain and composition has not been optimized for MRI contrast. As the difference in relaxivity between the disrupted and intact states of Mn porphysomes suggests, water access to the coordination shell of the Mn ions is limited within the hydrophobic bilayer of the porphysome. Substitution of an unsaturated lipid chain into Mn pyro-lipid or the inclusion of cholesterol or a non-paramagnetic lipid into the formulation may favourably alter the membrane. Characteristics such as water permeability (which primarily affects r_1) and membrane fluidity/Mn-ion clustering (which primarily affects r_2) give further avenues for optimizing the MR properties of Mn porphysomes.

This study illustrates the flexibility of forming nanoparticles from a single, multimodal building block in a one-for-all approach. The insertion of Mn into pyro-lipid was fast and quantitative and the formulation of porphysomes was comparable to that previously reported for free-base porphysomes. The insertion of Mn^{3+} ions into the porphyrin rings renders porphysomes capable of generating MRI contrast at a level comparable to the clinically used Gd-DTPA while synergistically improving upon the already potent photothermal capabilities of free-base porphysomes, all while maintaining the simplicity of the system.

Received: January 6, 2014
Revised: March 20, 2014
Published online: May 19, 2014

Keywords: manganese · nanoparticles · photostability · porphyrins · theranostics

[1] a) G. Jori, J. D. Spikes, *J. Photochem. Photobiol. B* **1990**, *6*, 93–101; b) J. A. Parrish, R. R. Anderson, T. Harrist, B. Paul, G. F. Murphy, *J. Invest. Dermatol.* **1983**, *80*, S75–S80.

 © 2014 Wiley-VCH Verlag GmbH & Co. KGaA, Weinheim

[2] a) A. J. Welch, *IEEE J. Quantum Electron.* **1984**, *20*, 1471 – 1481; b) C. Sturesson, S. AnderssonEngels, *Phys. Med. Biol.* **1995**, *40*, 2037 – 2052.
[3] M. Longmire, P. L. Choyke, H. Kobayashi, *Nanomedicine* **2008**, *3*, 703 – 717.
[4] H. Maeda, J. Wu, T. Sawa, Y. Matsumura, K. Hori, *J. Controlled Release* **2000**, *65*, 271 – 284.
[5] a) X. H. Huang, I. H. El-Sayed, W. Qian, M. A. El-Sayed, *J. Am. Chem. Soc.* **2006**, *128*, 2115 – 2120; b) X. H. Huang, P. K. Jain, I. H. El-Sayed, M. A. El-Sayed, *Laser Med. Sci.* **2008**, *23*, 217 – 228.
[6] N. Khlebtsov, L. Dykman, *Chem. Soc. Rev.* **2011**, *40*, 1647 – 1671.
[7] a) C. S. Jin, J. F. Lovell, J. Chen, G. Zheng, *ACS Nano* **2013**, *7*, 2541 – 2550; b) J. F. Lovell, C. S. Jin, E. Huynh, H. Jin, C. Kim, J. L. Rubinstein, W. C. Chan, W. Cao, L. V. Wang, G. Zheng, *Nat. Mater.* **2011**, *10*, 324 – 332.
[8] J. Cepek, B. A. Chronik, U. Lindner, J. Trachtenberg, S. R. Davidson, J. Bax, A. Fenster, *Med. Phys.* **2013**, *40*, 012304.
[9] a) U. Lindner, S. R. H. Davidson, M. A. Haider, E. Hlasny, M. R. Gertner, B. C. Wilson, W. Kucharczyk, J. Trachtenberg, *Eur. Urol. Suppl.* **2012**, *11*, E15 – U320; b) U. Lindner, R. A. Weersink, M. A. Haider, M. R. Gertner, S. R. H. Davidson, M. Atri, B. C. Wilson, A. Fenster, J. Trachtenberg, *J. Urol.* **2009**, *182*, 1371 – 1377; c) O. Raz, M. A. Haider, S. R. H. Davidson, U. Lindner, E. Hlasny, R. Weersink, M. R. Gertner, W. Kucharcyzk, S. A. McCluskey, J. Trachtenberg, *Eur. Urol.* **2010**, *58*, 173 – 177.
[10] A. Y. Louie, *Chem. Rev.* **2010**, *110*, 3146 – 3195.
[11] a) T. W. Liu, T. D. MacDonald, C. S. Jin, J. M. Gold, R. G. Bristow, B. C. Wilson, G. Zheng, *ACS Nano* **2013**, *7*, 4221 – 4232; b) T. W. Liu, T. D. MacDonald, J. Shi, B. C. Wilson, G. Zheng, *Angew. Chem.* **2012**, *124*, 13305 – 13308; *Angew. Chem. Int. Ed.* **2012**, *51*, 13128 – 13131.
[12] a) D. P. J. Pan, S. D. Caruthers, A. Senpan, A. H. Schmieder, S. A. Wickline, G. M. Lanza, *Wires Nanomed. Nanobiol.* **2011**, *3*, 162 – 173; b) T. Lee, X. A. Zhang, S. Dhar, H. Faas, S. J. Lippard, A. Jasanoff, *Chem. Biol.* **2010**, *17*, 665 – 673; c) X. A. Zhang, K. S. Lovejoy, A. Jasanoff, S. J. Lippard, *Proc. Natl. Acad. Sci. USA* **2007**, *104*, 10780 – 10785.
[13] N. C. Tam, P. Z. McVeigh, T. D. MacDonald, A. Farhadi, B. C. Wilson, G. Zheng, *Bioconjugate Chem.* **2012**, *23*, 1726 – 1730.
[14] a) Y. G. Wang, K. J. Zhou, G. Huang, C. Hensley, X. N. Huang, X. P. Ma, T. Zhao, B. D. Sumer, R. J. DeBerardinis, J. M. Gao, *Nat. Mater.* **2014**, *13*, 204 – 212; b) C. S. Jin, L. Cui, F. Wang, J. Chen, G. Zheng, *Adv. Healthcare Mater.* 10.1002/adhm.201300651; c) K. K. Ng, J. F. Lovell, A. Vedadi, T. Hajian, G. Zheng, *ACS Nano* **2013**, *7*, 3484 – 3490.
[15] a) A. Harriman, *J. Chem. Soc. Faraday Trans. 1* **1980**, *76*, 1978 – 1985; b) A. Harriman, *J. Chem. Soc Faraday Trans. 2* **1981**, *77*, 1281 – 1291.
[16] J. L. Sessler, T. D. Mody, G. W. Hemmi, V. Lynch, S. W. Young, R. A. Miller, *J. Am. Chem. Soc.* **1993**, *115*, 10368 – 10369.

 © 2014 Wiley-VCH Verlag GmbH & Co. KGaA, Weinheim